Journal of Controlled Release 309 (2019) 265–276

Contents lists available at ScienceDirect

Journal of Controlled Release

journal homepage: www.elsevier.com/locate/jconrel

pH-responsive poly(lactide-*co*-glycolide) nanoparticles containing near-infrared dye for visualization and hyaluronic acid for treatment of osteoarthritis

L. Zerrillo[a,b], I. Que[a], O. Vepris[a], L.N. Morgado[c,i], A. Chan[b], K. Bierau[b], Y. Li[b], F. Galli[d], E. Bos[e], R. Censi[f], P. Di Martino[f], G.J.V.M. van Osch[g], L.J. Cruz[a,*]

[a] Translational Nanobiomaterials and Imaging (TNI) Group, Radiology Department, Leiden University Medical Centrum, Leiden, The Netherlands
[b] Percuros, Enschede, The Netherlands
[c] Section for Genetics and Evolutionary Biology (EVOGENE), Department of Biosciences, University of Oslo, Oslo, Norway
[d] Leiden Institute of Physics, Niels Bohrweg 2, Leiden, The Netherlands
[e] Department of Molecular Cell Biology, Section Electron Microscopy, Leiden University Medical Center, Leiden, The Netherlands
[f] University of Camerino, School of Pharmacy, Italy
[g] Department of Orthopedics and Department of Otorhinolaryngology, Erasmus MC University Medical Centre, Rotterdam, The Netherlands
[i] Naturalis Biodiversity Center, Leiden, The Netherlands

ARTICLE INFO

Keywords:
pH-sensitive nanoparticles
PLGA
Hyaluronic acid
Drug delivery
Intra-articular injection
Molecular imaging

ABSTRACT

This study focuses on intra-articular (IA) drug delivery system for the treatment of knee osteoarthritis (OA). In osteoarthritic condition the synovial fluid presents pockets with lower pH environment. To take advantage of these pH differences, poly(lactic-*co*-glycolic acid (PLGA) nanoparticles (NPs) and pH– responsive PLGA NPs encapsulated with ammonium bicarbonate (NH_4HCO_3) were generated. The nanoparticles were loaded with hyaluronic acid (HA) as a possible model drug for OA and with near-infrared dye (NIR) that was used to visualize the NPs with molecular imaging techniques. These NPs were characterized by dynamic light scattering, transmission electron microscopy and compared in *in vitro*, *in vivo* and *ex vivo* experiments in the treatment of OA. The results indicate that the NPs were sufficiently small, displayed a uniform size distribution and were non-toxic both *in vitro* and *in vivo*. Both NPs treatment seem to induced a reduction in OA progression, with pH- responsive NPs showing the more pronounced effect. This is probably because the pockets of low pH environment in the synovial fluid trigger a burst release of the pH-responsive NPs. This result is corroborated by *in vitro* experiments since the pH- responsive NPs showed an extracellular burst release behavior and higher chondrocyte vitality than non-responsive NPs. This study demonstrates that PLGA NPs containing HA and NH_4HCO_3 are candidates for the treatment of knee OA.

1. Introduction

Osteoarthritis (OA) is the most prevalent degenerative joint disorder and affects mainly the knee, the hip and the small joints in the hand [1]. It is characterized by the degeneration of articular cartilage, subchondral bone sclerosis, osteophyte formation, synovial inflammation and hypertrophy of the joint capsule [2,3]. The pathological changes in these tissues lead to progressive functional limitations, chronic pain with reduced quality of life and, ultimately, joint failure [4]. Currently there is no cure for OA. General guidelines for the management of OA, before the final stage, which involves the joint replacement, are divided according to the OA stage classification [5]. In an initial stage, there is a focus on non-pharmacological and non-surgical measures involving specific physical exercises and body weight control/loss. With the augmentation of patient pain, the initial stage treatment is supplemented with drug administration. Pharmacological treatments are mainly palliative targeting pain reduction in early stage of OA. The most common drugs used are acetaminophen, non-steroidal anti-inflammatory drugs, tramadol, intra-articular injection of corticosteroid and hyaluronic acid (HA), *i.e.*, viscosupplementation [6,7].

In OA joints the HA present in synovial fluid is degraded by reactive oxygen species (ROS) inducing lower concentration of HA causing

* Corresponding author at: Translational Nanobiomaterials and Imaging, Department of Radiology, Bldg.1, C2-187h, Leiden University Medical Center, Albinusdreef 2, 2333 ZA Leiden, The Netherlands.
E-mail address: l.j.cruz_ricondo@lumc.nl (L.J. Cruz).

https://doi.org/10.1016/j.jconrel.2019.07.031
Received 13 February 2019; Received in revised form 17 June 2019; Accepted 20 July 2019
Available online 27 July 2019
0168-3659/

lower viscosity and reduced shock protection [8–10]. Artificially increasing the HA concentration helps patients to restore the viscoelasticity of the synovial fluid (SF) and relieves pain [11–13]. HA has also been suggested to induce biological changes such as moderation of inflammation, reduction of cytokine-induced enzyme production, antioxidant action, anabolizing effect on cartilage, and direct analgesia by masking the joint nociceptors [14,15]. CD44 is the primary receptor for HA. HA-CD44 interaction is essential for the normal homeostasis of the cartilage [16,17], since it can modulate cartilage metabolism and promote matrix remodeling of the cartilage [18,19]. There is an ongoing database on the effects of HA in OA, in a review on the subject, Rutjes et al. [20] concluded that there is a small and clinically irrelevant benefit while Santilli et al. [21] and Maheu et al. [22] concluded that intra-articular injection of HA results in long-lasting improvements in function, including the potential to avoid a joint prosthetic implant and pain reduction. Additionally, repeated intra-articular injections of HA have been shown to relief pain and improve joint function with the effects persisting for up to 26 weeks [23]. However, the rapid clearance from the joint by the synovium requires frequent intra-articular injections, which may result in complications, such as infections [24].

There is a growing interest in the modernization of OA therapeutics to improve treatment efficacy. As a response, there has been significant developments, particularly through targeted therapeutics, such as nanoparticles (NPs) therapeutics [25,26]. NPs are nanoscale vectors made of biocompatible and biodegradable polymers enclosing small therapeutic entities (small-molecule drugs) with high potential for targeted therapy. NPs are typically stable over extended periods, and can be loaded with both hydrophilic and hydrophobic compounds. The payload release can be controlled and actively targeted to specific cells, organs or tissues [27]. Poly lactic-*co*-glycolic acid (PLGA) is one of the most commonly used co-polymers in drug delivery. The polymers used to form PLGA, lactide and glycolide, are endogenous and metabolized by enzymes in the Krebs cycle [28]. Moreover, PLGA is FDA approved [29] and can be readily used in clinical applications. Another advantage of using NPs is the possibility to co-load the desired drugs with fluorescent dye. This dye functions as a probe and allows the researchers to trace and infer NPs therapeutics efficiency through molecular imaging. These probes are small molecules that typically have a molecular weight of a few hundred Da, they are non-toxic and can be tissue specific. OA treatment can benefit from intra-articular injection of nanomaterials, for example, through controlled drug release *in vivo* and high efficiency at low concentrations with the aim to inhibit progression of cartilage damage [30,31]. Indeed, Zille et al. [25] in an *in vivo* study showed that intra-articular injections of PLGA NPs covered with HA are safe for drug delivery in OA since they found no tissue function modifications not inflammatory response between treatment and control rats that were subjected to NPs injection.

The objectives of this work were twofold, *i.e.* first to investigate the effect of pH on NPs therapy, and second to study the effect of HA-loaded NPs on OA in the knee. NH_4HCO_3 was chosen to be co-loaded into the NPs because previous studies showed that in different areas of the synovial cavity there is a decrease of the synovial fluid pH [32], it is however unclear the extent of these areas in the synovial fluid. Nevertheless, this can be used to enhance drug effectiveness, since the porous surface of PLGA NPs permits the entrance of small molecules like H_2O and H_3O^+. The high concentration of hydronium ions (H_3O^+), present at low pH, react with NH_4HCO_3 loaded in the NPs, inducing a pH neutralization with the production of NH_4^+, CO_2 and H_2O. This conversion results in the breakdown of the NPs shell, causing a burst release. Liu and colleagues [33] used a similar method to successfully generate pH-response PLGA NPs for the treatment of intracellular infectious diseases and virus infection, showing that this method may be effective in vaccine delivery.

2. Materials and methods

2.1. Materials

PLGA (Resomer RG 502H, lactide:glycolide molar ratio 48:52 to 52:48) was purchased from Boehringer Ingelheim (Germany). Polyvinyl alcohol (PVA) (87–89% hydrolyzed, typical MW 13.000–23.000), Hyaluronic acid sodium salt (HA) Mw 750,000-1000,000 and ammonium bicarbonate (NH_4HCO_3) (AB) were purchased from Sigma Aldrich (Stenheim, Germany). The solvent for PLGA NPs preparation dichloromethane (DCM), was purchased from Sigma Aldrich (Stenheim, Germany). The NPs were all loaded with NIR dye (IR-780 Iodide) purchased from Sigma-Aldrich (Zwijndrecht, The Netherlands). The *in vitro* studies were performed using The CellTiter 96® AQueous One Solution Cell Proliferation Assay Promega, Dulbecco's Modified Eagles Medium ThermoFisher SCIENTIFIC, To-pro 3 iodide (642/661) Invitrogen (Eugene, USA).

2.2. Rational design of NPs

The pH- responsive PLGA NPs AB experimental design is illustrated in Fig. 1. NPs were synthesized by the emulsion-solvent evaporation method and loaded with NIR dye, HA and NH_4HCO_3. HA was used as model drug for OA and NH_4HCO_3 was used to induce the burst release of pH-response PLGA NPs AB. NIR allows the traceability of the NPs by optical imaging. NPs were injected intra-articularly in mice 3 weeks after surgery for the destabilization of medial meniscus (DMM). The molecules of H_3O^+, present in pockets of the SF with low pH, penetrate the porous shell of PLGA NPs and react with NH_4HCO_3 generating NH_4^+, CO_2 and H_2O inducing the NPs shell collapse releasing the entrapped HA.

2.3. Preparation of control PLGA NPs

Control PLGA NPs, from here onwards referred to as PLGA NPs, were prepared by single emulsion-solvent evaporation method to reduce the particle size to submicron size range. The polymers PLGA and NIR (IR-780 Iodide) were dissolved in DCM and emulsified in water phase containing an emulsifying agent PVA 0.5%. The emulsion was continuously stirred at 24.000 rpm using a mechanical stirring system (ULTRA-TURRAX T25, IKA, Staufen, Germany) until the organic solvent partitioned into the aqueous phase and then evaporated. The emulsion formed was stirred under magnetic stirring (IKA® RCT basic IKAMAG™, Germany) for > 20 min to completely evaporate the solvent. The suspension formed contained polydisperse NPs. The NPs were washed four times with MilliQ water to remove excess of PVA that could interfere with the morphology and the toxicity of the NPs. The NPs were washed by centrifugation at 14.000 rpm, 4 °C for 30 min. The resulting pellet containing the NPs was re-suspended in MilliQ water and lyophilized.

For the preparation of PLGA NPs loaded with Fluorescein isothiocyanate (FITC) dye, a similar protocol as the one described above for the NIR dye was used with the exception that 0.5 mg of FITC dye were initially dissolved in MilliQ water.

2.4. Preparation of PLGA NPs with and without ammonium bicarbonate containing hyaluronic acid

To test NPs response to environment pH, two types of NPs were generated, (1) not pH-responsive NPs, containing HA, from here onwards referred to as PLGA NPs A, and (2) pH-responsive NPs containing HA and NH_4HCO_3, from here onwards referred to as PLGA NPs AB. Both NPs were generated with double emulsion-solvent evaporation method, water-oil-water. The oil phase containing the PLGA and NIR was added drop-by-drop to the first water phase containing HA and NH_4HCO_3 dissolved in MilliQ water. The emulsion was mechanical stirred for five

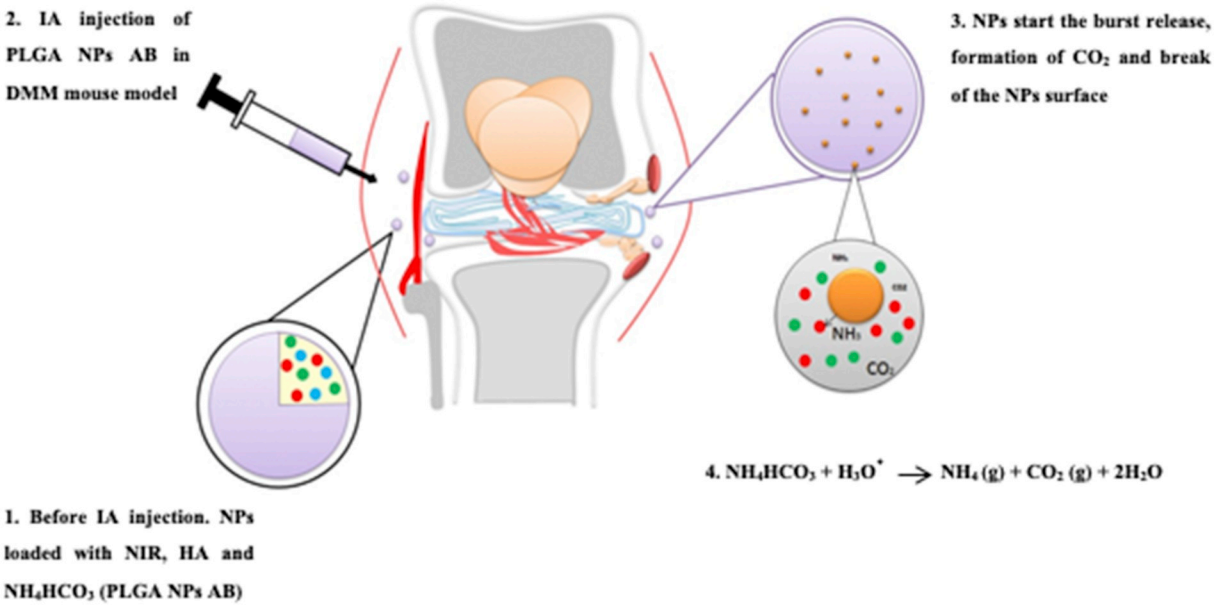

Fig. 1. Schematic illustration of the methodology used to generate pH-responsive PLGA NPs (AB). NPs were encapsulated with NIR dye for optical imaging purposes, Hyaluronic acid, used as model drug for OA, and NH_4HCO_3, used to induce the burst release of pH-response PLGA NPs AB.

minutes with Ultra- Turrax (IKA, Staufen, Germany). The water to oil emulsion formed was then added drop-by-drop to the second water phase containing PVA 0.5% as emulsifying agent. The water-oil-water emulsion was continuously stirred at 24.000 rpm for 20 min with an Ultra-Turrax until the organic solvent was partitioned into the aqueous phase and then evaporated. The suspended NPs formed were magnetically stirred (IKA® RCT basic IKAMAG™, Germany) for 20 min at moderate speed to ensure the complete evaporation of the solvent. The suspension formed, containing polydisperse NPs, was separated by ultracentrifugation at the speed of 14.000 rpm for 30 min at 4 °C. The NPs were washed four times with MilliQ water to remove any excess of PVA. NPs were re-suspended in MillQ water and lyophilized. For the preparation of PLGA NPs A and PLGA NPs AB loaded with FITC dye, a similar protocol as the one described above for the NIR dye was used with the exception that 0.5 mg of FITC dye were initially dissolved in of MilliQ water.

2.5. Encapsulation efficiency analysis of NIR dye

In order to determine encapsulating efficiency (EE) and loading content of the Near infrared dye (NIR), the lyophilized NPs were first dissolved in 0.8 M NaOH. Separately, 5 mg of PLGA NPs, PLGA NPs A and PLGA NPs AB were dissolved in 0.5 mL 0.8 M NaOH solution overnight at 37 °C. Afterwards, the solutions of all the NPs were centrifuge at 12.000 rpm for 20 min at room temperature and the supernatants were collected. The dye content was then measured using Odyssey Infrared Imager 9120 (LI-COR) scanner with an 800 nm scan. NIR dye encapsulation efficiency was calculated using the following formula, previously described in [34]:

$$EE = \frac{Amount\ of\ drug\ in\ formulation}{Amount\ of\ drug\ used\ for\ formulation} x100 \quad (1)$$

Amount of drug in formulation is the amount of NIR loaded in the NPs, measured with Odyssey Infrared Imager, while the *amount of drug used for formulation* is the amount of NIR dye added in the preparation of NPs.

2.6. Encapsulation efficiency analysis of FITC dye

For the quantification of Fluorescein isothiocyanate (FITC) dye, 5 mg of dry NPs were dissolved in 0.8 M NaOH, as above described. The separate solutions contained PLGA NPs, PLGA NPs A and PLGA NPs AB, were centrifugated at 12.000 rpm for 20 min at room temperature and the supernatants were collected. The FITC dye content was then measured with Amersham Biosciences ultrospec 2100 pro, UV/Vis Spectrophotometer. The amount of FITC dye was calculated by the slope of the standard curve obtained by the linear regression for FITC concentration.

2.7. Quantification of HA loading

HA loading into NPs was quantified by cetyltrimethylammonium bromide turbidimetric assay (CTAB-method). CTAB is a cationic surfactant that precipitates polyanionic HA. The amounts of HA loaded into the PLGA NPs A and PLGA NPs AB were quantified after hydrolyzing 5 mg of the NPs in 0.5 mL 0.8 M NaOH solution overnight at 37 °C. The CTAB method was described elsewhere, Oueslati et al. [35]. Briefly, CTAB was dissolved in 100 mL of 2% NaOH; 50 µL of HA standard solution and the supernatant of PLGA NPs A and PLGA NPs AB, were added into a 96 well plate previously filled with 50 µL of 0.1 M phosphate buffer at pH 7 and incubated for 15 min at 37 °C. Then, 100 µL of CTAB reagent were added to each well and the plate was incubated for 10 min at 37 °C. Absorbance was read at 600 nm with Molecular Devices VERSAmax Tunable Microplate Reader (Software used SoftMAX Pro v5.4.1). The amount of HA was calculated by the slope of the standard curve obtained by the linear regression for HA concentration.

2.8. Physicochemical characterization of NPs

2.8.1. Particles size and charge surface

The average size and polydispersity index (PDI) of the NPs were determined by Dynamic Light Scattering (DLS) (Zetasizer Nano S90, Malvern Instruments, Worcestershire, UK). NPs were dissolved in MilliQ water and measured at 25 °C at 90° angle. The values presented are averages and standard deviations of triplicated measurements. The stability and aggregation in NPs dispersion was determined by Zeta potential (Zetasizer Nano S90, Malvern Instruments, Worcestershire, UK) (Table 1).

Table 1
NPs size, polydispersity, zeta potential, NIR dye, FITC dye drug encapsulation efficiency (EE) of PLGA NPs, PLGA NPs A and PLGA NPs AB.

Nanoparticles	Particles size (nm)	Polydispersity	Zeta potential (mV)	EE% (NIR)	EE% (FITC)	EE% (HA)
PLGA NPs	159 ± 0.98	0.226 ± 0.01	−18.9	20.3	20.3	–
PLGA NPs A	175 ± 0.51	0.070 ± 0.01	−17.6	10.8	14.8	46.5
PLGA NPs AB	202.7 ± 2.3	0.225 ± 0.03	−21.0	3.2	4.4	28.1

2.8.2. Particles surface and morphology

Surface morphology and size of optimized PLGA NPs AB was studied with atomic force microscopy (AFM). PLGA NPs AB were first diluted and dispersed in MilliQ water. Then a drop of the suspension was placed on a clean glass surface glued to the AFM stub and air dried for one hour. The dried NPs were then visualized with AFM (JPK Nano Wizard 3) in AC mode (tapping mode) using OMCL-AC160TS silicon probes (Olympus, City, Country) with nominal resonance frequency of 300 kHz and nominal spring constant of 26 N/m. The images were analyzed using Gwyddion SPM Software (Supported by Department of Nanometrology, Czech Metrology Institute (Brno, CZ)). The 2D visualization was performed in JPK Data Processing Software, JPK Instruments, Berlin (DE) and the images were then converted to 3D using Gwyddion, Open Source SPM Data Analysis Software.

To visualize and characterize particle size, size distribution and morphology of all the NPs, transmission electron microscopy was used. A formvar support film attached to a copper grid (100 mesh) was coated with carbon and hydrophilized by glow-discharging for 30 s with a current of 25 mA. A droplet of 3 μL of the particle solution was applied to the grid for 1 min after which the excess suspension was removed by blotting. The grid was then stained for 1 min in distilled water containing 2.3% uranyl acetate, after which, excess staining solution was removed by blotting. Subsequently, the grid was air-dried and imaged in a Tecnai 12 Biotwin transmission electron microscope (FEI, the Netherlands), equipped with a LaB6 filament operated at 120 keV. The sample was imaged at 3 μm under focus with binning 2 on a 4kx4k Eagle CCD camera with a magnification of 18,500×.

2.9. Release characterization

2.9.1. Quantification of HA released from PLGA NPs A and PLGA NPs AB

The HA released from PLGA NPs A and PLGA NPs AB were quantified by cetyltrimethylammonium bromide turbidimetric assay (CTAB). Five mg of freeze-dried NPs, were resuspended in 5 mL saline phosphate buffer at pH 7.4 and pH 5.0 at 25/26 °C under mild agitation. After 20 min of centrifugation at 12.000 rpm, 150 μL of the supernatant were collected and replaced with fresh 150 μL of PBS with the respective pH (7.4 and 5.0). This procedure was performed at different time points: 1, 2, 3, 4, 5, 8 and 10 days.

2.9.2. 30 days release study at different pH of NIR dye

The release study of NIR dye at different pH's was performed with 5 mg of freeze-dried NPs. The NPs were resuspended in 5 mL saline phosphate buffer at pH 7.4 and pH 5.0 at 25/26 °C under mild agitation. After 20 min of centrifugation at 12.000 rpm, 150 μL of the supernatant was collected and replaced by 150 μL of fresh PBS with the respective pH (7.4 and 5.0). This procedure was performed at different time points: 1, 2, 7, 15, 20, 23, 26 and 30 days. The NPs released and present in the supernatant were quantified by Odyssey™ scanner using the 800 nm channel for visualization of NIR dye.

2.9.3. 20 days release study in synovial fluid of NIR dye

For each of the NPs (PLGA NPs, PLGA NPs A, PLGA NPs AB), the release study of NIR dye was performed in human synovial fluid (SF) and measured at 8 time points, 1, 2, 5, 7, 9, 11, 15 and 20 days. The synovial fluid was obtained from anonymous patients that were subjected to knee replacement surgery at the Department of Orthopedic Surgery in Leiden University Medical Centrum. For this study, 0.5 mg of freeze-dry NPs were dissolved in 75 μL of SF and kept under mild agitation at 25/26 °C. At each time point, the solutions (NPs dissolved in the SF) were centrifuged for 20 min at 12.000 rpm at 4 °C, after which, 50 μL of the supernatant were collected and replaced by 50 μL of fresh SF. The supernatant NPs were quantified by Odyssey™ scanner using the 800 nm channel for visualization of NIR dye.

2.9.4. 24 h release study at pH 7.4 and 5 of NIR dye

To visualize the initial release of NIR dye, 20 μg of NPs were dissolved in PBS at pH 7.4 and 5.0 and, incubated for 24 h at 37 °C in a culture slide (Chamber Polystyrene Vessel Tissue Culture Treated Glass Slide, FALCON). After the incubation, PBS solutions (pH 7.4 and 5.0) were removed from the chambers, coverslips were mounted using Acqua Poly/Mount (Polysciences) and examined by fluorescence microscopy. The wells containing the NPs were examined with a Leica DM5500 B fluorescence microscope (the filter settings were TXR, Cy7, FITC and DAPI) equipped with a Leica DFC365 FX digital camera. Digital images were acquired and stored using Leica Application Suite X (LAS X) software.

2.10. In vitro experiment

2.10.1. Cell culture

Human chondrocyte cell line C28/I2 were kindly donated from M. Goldring. The cells were cultured in 75 cm flasks in 1:1 Dulbecco's Modified Eagles Medium (DMEM) /F12 medium (Gibco Cell Culture Medium, ThermoFisher Scientific) with 10% (*v*/v) fetal calf serum (FCS; Life technology) at 37 °C, atmosphere of 95% air and 5% CO_2. Every 48 h the medium was changed. The cells were sub-cultured for experiments after growing to approximately 80–90% confluence [36,37].

2.10.2. Cell metabolic assay (MTS)

Effects of NPs and free HA on cell behavior were investigated using human chondrocytes cell line C28/I2. The MTS assay was performed using 5×10^4 cells/well in 96 well plates. After 24 h incubation at 37 °C the NPs suspensions were added to the cells at different concentrations: 10, 20, 40 and 60 μg/mL. The free HA was added at the concentration standardized to the encapsulation efficiency relative to the respective PLGA NPs AB concentrations. The cellular metabolic activity was studied over incubation periods of 24, 48 and 72 h. To establish a positive cytotoxicity control, cells were treated with 50% DMSO. Non-treated cells were used as negative control. Subsequently, 20 μL of [3-(4,5-dimethylthiazol-2-yl)-5-(3-carboxymethoxyphenyl)-2-(4-sulfophenyl)-2H-tetrazolium (MTS) (Promega, The Netherlands) were added to each well and incubated for 1 h at 37 °C. The absorbance was measured with a spectrophotometer at λex 590 nm (Molecular Devices VERSAmax Tunable Microplate Reader, LUMC). The assay was assessed according to manufacturer's instructions. The cell's metabolic activity in each condition was expressed as increased percentage in relation to untreated controls.

2.11. NPs up-take studies

2.11.1. Up-take studies of NPs and characterization by flow cytometry

The C28/I2 cells were seeded in 96 well cell culture microplate (Greiner Bio-One B.V., The Netherlands) (2.5×10^4 cells/well)

incubated with 40 μg/mL of PLGA NPs, PLGA NPs A, PLGA NPs AB, for 1, 2, 4, and 24 h. All the NPs were incapsulated with FITC dye. After incubation, the cells were washed twice with FACS buffer (PBS with 0.5% BSA and 0.02% sodium). All flow cytometric analyses were carried out on samples suspended in FACS buffer and FITC panel was used for the analysis on a BD LSR-II flow cytometer.

2.11.2. Up-take studies of NPs and characterization by odyssey infrared imaging system

The C28/I2 cells were seeded in 96 well cell culture microplate (Greiner Bio-One B.V., The Netherlands) (2.5×10^4 cells/well) incubated with 40 μg/mL of PLGA NPs, PLGA NPs A, PLGA NPs AB, for 1, 2, 4, and 24 h. After incubation, the cells were washed twice with PBS, fixed for 15 min with 2% paraformaldehyde in PBS, rinsed in PBS, and stained with To-pro 3 iodide dye, which stains the cell nucleus detectable at 700 nm. The plate was analyzed by Odyssey Infrared Imager 9120 (LI-COR) scanner using the 800 nm and 700 nm channel for visualization of NPs loaded with NIR and the cells, respectively.

2.11.3. Up-take studies of NPs and characterization by fluorescent microscopy

To visualize the up-take of NPs by cells after 24 h of incubation a supplemental experiment was performed. The C28/I2 cells were plated in a chamber plate (Falcon™ Chambered Cell Culture Slides) (2.5×10^4 cells/well) containing coverslips and co-incubated for 24 h with 40 μg/mL of PLGA NPs, PLGA NPs A, PLGA NPs AB. After incubation, the cells were washed twice with PBS, fixed for 15 min with 2% paraformaldehyde in PBS and rinsed in PBS. The cells membrane was stained with CD44-PE (CD44 Monoclonal Antibody (IM7), PE, eBioscience™) for 20 min at 37 °C and then covered with Vectashield mounting medium containing DAPI. Coverslips were mounted using Acqua Poly/Mount (Polysciences) and examined by fluorescent microscopy (Leica DMRA fluorescence microscopy, LUMC, University of Leiden).

2.11.4. Up-take studies of NPs and characterization by confocal microscopy

To assess intracellular uptake of the particles, C28-I2 were plated in Cellview™ dishes (Greiner Bio-one) at a density of 26,000 cells/cm^2 in DMEM/F-12 supplemented with 10% fetal bovine serum (FBS, Biowest), 0.2 mM ascorbic-2-phosphate (Sigma-Aldrich), and 100 U/mL penicillin and streptomycin (Gibco). Cells were cultured for 24 h in a humidified incubator at 37 °C with 5% CO_2. Subsequently the NPs were added to the cells at concentrations of 40 μg/mL and incubated for an additional 24 h period in non-supplemented DMEM/F-12. Cells were fixed with formalin for 20 min, followed by 0.2% PBS-Triton for 20 min, and blocking with 5% PBS-BSA for 30 min. Subsequently cells were stained with 2.5 μg/mL Phalloidin-TRITC (Sigma-Aldrich) and 100 ng/mL DAPI for 1 h. Between each step, cells were washed three times with 0.05% PBS-Tween. Images were acquired using a Leica SP8X confocal microscope (Leica) and both 20×/1.4 dry-objective and 63×/1.4 oil-immersion objective. Image processing and analysis was performed using Fiji (National Institutes of Health, Bethesda, USA) software version 1.50.

2.12. Animals osteoarthritis model and experimental design

For the *in vivo* test, a total of 18 male C57BL/6Jico 12 weeks old mice were purchased from Charles River, France. From these, 3 mice were kept healthy and used as negative control. The remaining 15 mice were operated with surgical destabilization of medial meniscus (DMM) on the right knee, while the left knee was used as contralateral control [38]. After DMM, 3 mice were kept as positive control and received no NPs. At the end of the experiment, the positive controls mice were sacrificed to confirm knee OA and damage stage with Safranin-O/Fast green staining (supplementary material). The remaining 12 mice were evenly separated into 3 groups, to which 8 μL in intra-articular injections were administered with respectively 2.5 mg/mL (1) PLGA NPs (control NPs), (2) PLGA NPs A (NPs co-loaded with HA), and (3) PLGA NPs AB (NPs co-loaded with HA and NH_4HCO_3). These mice were sacrificed 35 days after receiving the NPs injections and the lower limbs were analyzed by μCT-scan. The limbs were fixed for 24 h in 4% buffered formaldehyde and subsequently decalcified in 14% EDTA for 3 weeks before using for *ex vivo* characterization. The animal procedures were all conducted in Leiden University Medical Centrum and approved by the Animal Welfare Committee of the Leiden University Medical Center approved the experiments under number 12036.

2.13. Retention time in the joint

The *in vivo* imaging system IVIS Spectrum (Perkin Elmer, Waltham,USA) was used to measure the retention time of fluorescent NPs in the knee joint. The mice were anesthetized using isoflurane. The imaging data were analyzed using the Living Image 4.3.1 software (Perkin Elmer, Waltham, USA). The fluorescence images were acquired with the use of a 710 nm excitation filter and 760, 780, 800, 820 and 840 nm emission filters. Both hind limbs were scanned to control for background tissue fluorescence. The NPs were followed for a total of 35 days. The NPs retention in the mice knee joint were followed through IVIS after 1, 24 and 48 h of intra-articular injection of NPs and after 7, 14, 21, 28 and 35 days.

2.14. μCT

To visualize the knee joint the SkyScan 1076 μCT scanner (Bruker, Kontich, Belgium) was used after sacrificing the mice. The hind limbs were fixed in formalin and scanned with 40 kV and 250 uA with an X-ray source rotation step size of 0.8° over 180°. Images were taken with an image pixel resolution of 9.03 μm and a frame averaging of 4 to reduce noise. Reconstructions were made using the nRecon V1.6.2.0 software (Bruker) with a beam hardening correction set to 25%, a ring artifact correction set to 5, and the dynamic range set to −1000–4000 Hounsfield units. 3D visualizations were made with software Cyttron Visualization Platform (LUMC, Leiden, NL).

2.15. Histological analysis

After optical imaging and μCT scan examinations, the limbs were fixed with 4% phosphate-buffered paraformaldehyde for 24 h, decalcified with 10% ethylene diaminetetraacetic acid (pH 7.4) for 2 weeks, and then embedded in paraffin. The knee joints were sliced into 5 μm sections, stained with Safranin O/Fast green and Hematoxylin/ Eosin and examined by light microscopy to evaluate the cartilage damage of femur and tibia in knee joint. The joint degeneration was assessed with OARSI cartilage degeneration score in histological assessment of mouse [10]. Scoring was performed by two independent researchers, blinded to the conditions and to the scores of the other investigator. The results were averaged and the OA score of the sections was taken as the representative score of the knee joint as described elsewhere [39].

2.16. Statistical analysis

With the exception of the *in vivo* study, all experiments were performed in triplicate. Results were expressed as means and standard deviations. Data were analyzed by *t*-test and two-way analysis of variance (ANOVA) using GraphPad Prism 5 software (CA, USA).

3. Results and discussion

3.1. Preparation and characterization of NPs

In this study, PLGA NPs were designed to be pH-responsive. The double emulsion-solvent evaporation method was successfully

performed to generate pH-responsive PLGA NPs (AB), which showed a burst release fashion profile. This method allowed quantification and optimization of drug encapsulation with a concomitant control of the NPs size. Previously, most studies focusing on NPs burst release profile applied methodologies aiming at the ligation of compounds to the surface of the NPs, either with Van der Waals bounds or covalent bounds. However, both these methods present limitations. The first method is made of an instable bound between the surface of the NPs and the compounds, which may lead to the loss of compounds when the NPs are in solutions, while the latter has an unstable attachment of the material on NPs surface [40–42]. On-the-other-hand, the method applied in this study, is emerging in the field as a promising avenue for the future research in NPs therapy, since the compounds are entrapped into the shell of the NPs reducing their potential loss in solution.

The average size of PLGA NPs (control) was 159 ± 0.98 nm, PLGA NPs A (non pH-responsive) was 175 ± 0.51 nm and PLGA NPs AB (pH-responsive) was 202.4 ± 2.30 nm in diameter (supplementary material Fig. 1D) (Table 1). The sizes of all the NPs are within the range of NPs able of active cellular uptake *via* endocytosis [43]. The NPs were all negatively charged as determined by Zeta potential. The NPs showed a good stability since the Zeta potential was between −23 mV and -17 mV values typically indicative of moderate to high NPs stability [44–46]. TEM analysis revealed that the NPs generated were all spherical with a smooth surface and uniform sizes (Fig. 2A). The morphology of the PLGA NPs AB was confirmed with AFM observations. The elongated shape of the particles depicted in Fig. 2B is an artifact due to microscope thermal drift. The sizes obtained by AFM were slightly smaller (Fig. 2B and Table 1) than those determined by DLS. The difference is likely due to different sample preparation methods since hydrated particles were used for DLS, whereas dehydrated NPs were used for AFM. The presence of HA loaded into PLGA NPs A and PLGA NPs AB was confirmed by ^{1}H NMR measures (supplementary material Fig. 1). ^{1}H NMR analysis further revealed that there were no traces of PVA in the NPs (supplementary material Fig. 2). The IR spectrum revealed that ammonium bicarbonate was successfully encapsulated in PLGA NPs AB and detectable after NPs formulation, thus proving that the compound was enclosed in the NPs (supplementary material Fig. 3). The encapsulation efficiency of fluorescent NIR for PLGA NPs was 20.3%, for PLGA NPs A 10.8% and for PLGA NPS AB 3.16% (Table1). The differences in encapsulation efficiency was probably because the single emulsion-solvent evaporation method (used to prepare the control NPs) has higher encapsulation efficiency than the double emulsion-solvent evaporation method (used to prepare PLGA NPs A and AB) [47]. The encapsulation efficiency of HA co-loaded for PLGA NPs A was 46.5% and for PLGA NPs AB, 28.1% (Table 1), indicating an acceptable encapsulation efficiency. There was a lower encapsulation efficiency of hyaluronic acid in PLGA NPs AB probably due to co-loading of NH_4HCO_3 which may constrain the NPs load capacity. Taken together these above results led to the conclusion that the generated NPs were safe and suitable for *in vivo* experiments.

3.2. In vitro release study at different pH values

The cumulative release study of HA and NIR dye was conducted in human synovial fluid and in both physiological and acidic pH conditions (pH 7.4 and 5.0, respectively), simulating the admixture pH of the synovial fluid environment in OA [32]. The results obtained clearly show that pH plays a critical role in the release of the drug encapsulated in the NPs.

In Fig. 3A and C, a cumulative release of HA and NIR dye at 7.4 pH shows similar release profile for all the NPs, *i.e.*, a constant release over time. Contrastingly, the cumulative release study of HA and NIR at pH 5.0 (Fig. 3B and D) showed that PLGA NPs AB after 2 days of incubation, released 80% of encapsulated HA, and reached 100% release after 8 days (Fig. 3B) while PLGA NPs and PLGA NPs A showed approximately half of the release percentage at the same time points. NIR dye was completely released after 2 days from PLGA NPs AB (Fig. D). The difference between NIR and HA release times are probably attributed the compounds molecular height. The results of the NIR release study in SF (Fig. 3E) showed a similar release profile for all the NPs up until the 5th day. After that time point, PLGA NPs AB had a faster release than the other NPs. This result yields similar conclusions as the release study in acidic PBS. The differences in the release time between SF and PBS media are probably due to differences in media density. Due to the lack of SF it was not possible to performed the release study of HA in SF medium.

The difference in release times of the different NPs was also visible by fluorescent microscopy, where the NIR dye of the pH- responsive NPs (PLGA NPs AB) (Fig. 3M) shows higher fluorescent intensity than the non-responsive pH NPs (Fig. 3I and L) due to a burst release of the pH-responsive NPs (PLGA NPs AB). The burst release happens because in acid environment, such as the SF in osteoarthritic condition, the hydronium ions (H_3O^+) are able to cross the shell of PLGA NPs and reacted with NH_4HCO_3 to produce NH_4^+, CO_2 and H_2O, increasing the inner pressure that eventually leads to the rapid rupture of the shell. After the initial 24 h, the pH-responsive NPs showed a considerably reduced release, while the non- responsive pH NPs showed a steady increase of release in acid pH environments (Fig. 3D). Collectively, the fluorescence microscopic images and the release profile graphic show that the PLGA NPs AB had a burst release up until 48 h and, that at 24 h the dye was still detectable indicating that the dye is still being released and, or, still did not degrade. Moreover, the NIR dye used to visualize

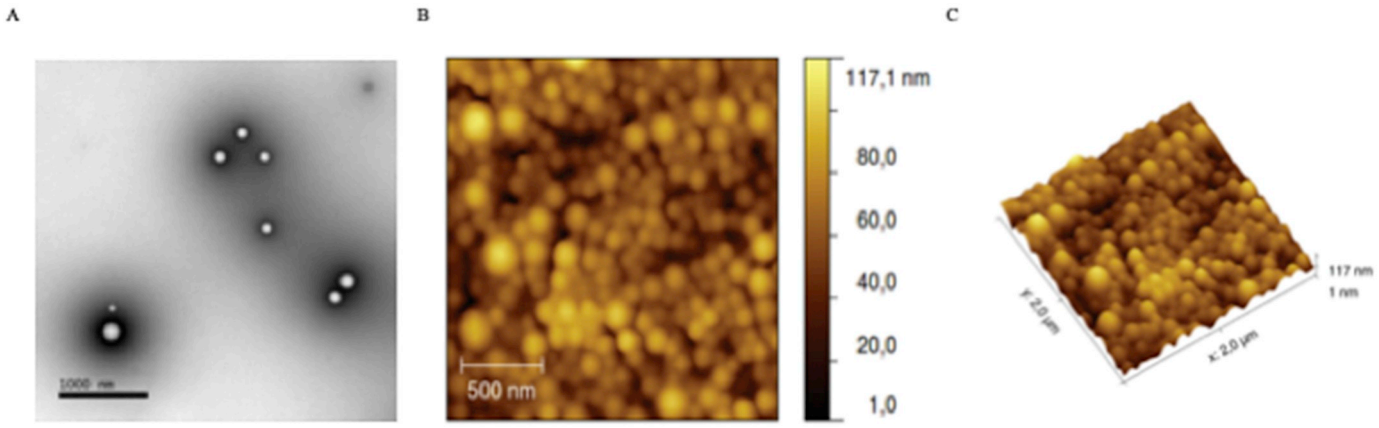

Fig. 2. Characterization of pH-response PLGA NPs AB with A) Morphology images of NPs obtained by TEM; B) AFM 2D image; C) and AFM 3D image of PLGA NPs AB.

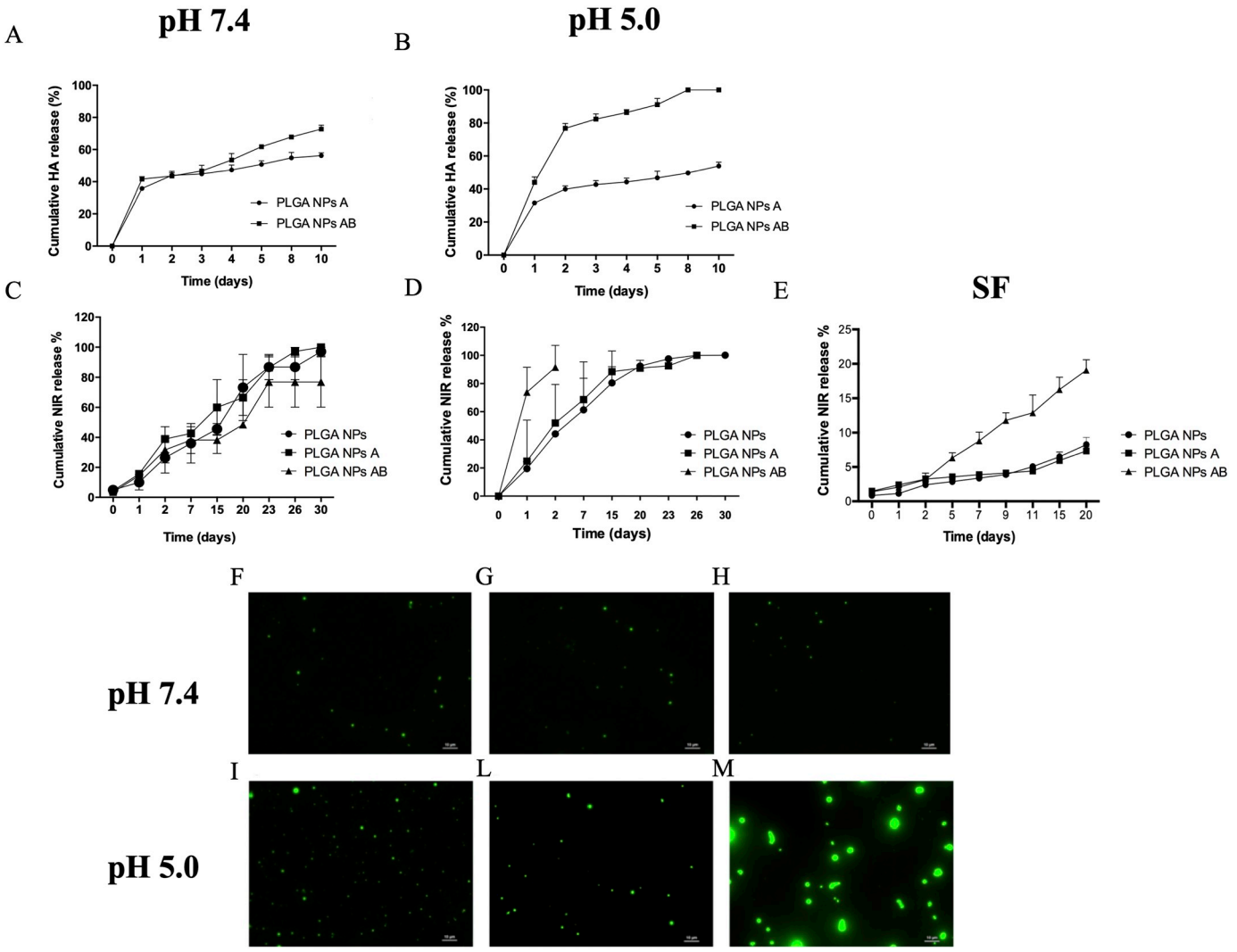

Fig. 3. Release study of HA and NIR dye from PLGA NPs A and PLGA NPs AB at different pHs. A) Cumulative release of HA in phosphate buffer followed for 10 days at pH 7.4 B) at 5.0. Statistical analysis showed significant differences for all the time points measured, except for the time point T0 ($p < .0001$). Cumulative release of fluorescent dye from NPs at different pHs. C-D) % cumulative release of NIR dye in phosphate buffer followed for 30 days at pH 7.4 (C) and 5.0 (D). E) Cumulative release of NIR dye in synovial fluid. F) PLGA NPs, G) PLGA NPs A and H) PLGA NPs AB. F-G—H) NPs were incubated for 24 h in PBS (pH 7.4) at 37 °C. I) PLGA NPs, L) PLGA NPs A and M) PLGA NPs AB. I-L-M) NPs were incubated for 24 h at pH 5.0. The images were made with Leica fluorescent microscopy at 63× magnification ($n = 3$).

all the NPs were non-target specific and showed similar wavelength absorption in both acidic and physiological pH media, indicating that the higher dye intensity observed for the pH- responsive NPs (PLGA NPs AB) was actually due to a burst release not due to other reasons, such as dye instability (supplementary material Fig. 4. A and B).

3.3. Characterization of the NPs in the in vitro experiments

3.3.1. Cellular metabolic assay

Cell metabolic activity was accessed with MTS assay. The assay was performed using a constant concentration (5×10^4 cells/well) of human chondrocyte cell lines C28/I2 and distinct concentration of NPs (10, 20, 40, 60 μg/mL) were measured at three different time points: 24, 48 and 72 h. Additionally, the effect of free HA with a concentration standardized to the encapsulation efficiency relative to the respective PLGA NPs AB concentrations were also measured. The metabolic activity assay revealed that, except PLGA NPs (control) at 60 μg/mL, all other NPs induced high cell viability after 72 h of incubation for all the concentrations. It is however interesting to note that comparing within NPs, the concentration of 60 μg/mL induced lower cell metabolic activity than lower concentrations at 72 h. The lower cell metabolic activity induced by PLGA NPs at 60 μg/mL at 72 h may be explained by the lack of loaded HA and by the non-degradation of the NPs. On the other hand, regardless of the NPs concentrations, at 72 h, PLGA NPs AB showed a significantly higher metabolic activity in comparison with the control PLGA NPs (Fig. 4). At the same time point, the highest metabolic activity was registered for PLGA NPs AB at the concentration of 40 μg/mL with a significant difference from all the other NPs. It was also observed that at 72 h the concentration of 60 μg/mL had the lowest metabolic activity among the experimented concentrations (Fig. 4C). It is worth mentioning that in an initial phase cell viability may be constrained by several reasons, such as cell growth and/or NPs compound release, which may act in synergy to the polymers composing the NPs shell. Indeed, PLGA is composed of two polymers, lactide and glycolide that are endogenous and metabolized by the Krebs cycle of cells [28]. After 3 days of incubation with cells, the PLGA starts to degrade and the

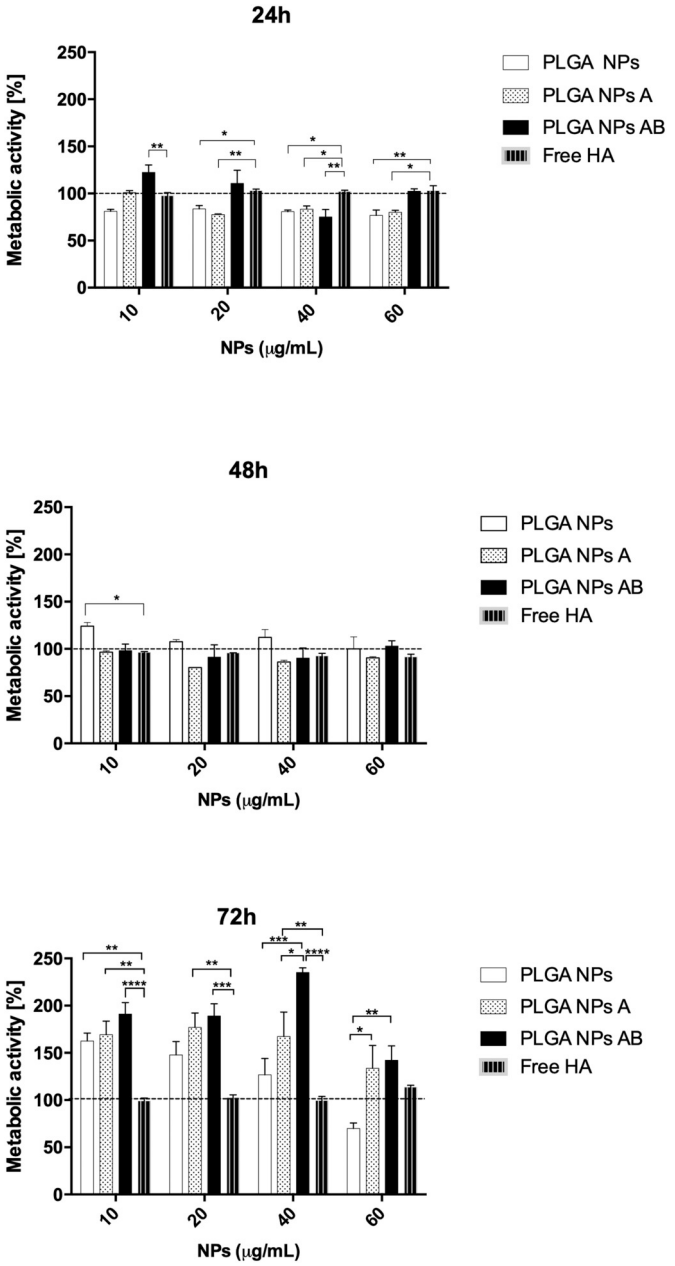

Fig. 4. Cell metabolic activity assay (MTS) of the 3 different NPs and free HA at different concentrations incubated with C28/I2 cell line. The percent of metabolic cell activity was measured at three time points: A) 24 h, B) 48 h, C) 72 h. For each assay the positive control was obtained using DMSO 50% and the negative control was obtained with only cells. The negative controls are indicated by the dashed horizontal line. Asterisks notation indicates significant difference in *t*-test, * $p < .05$, ** $p < .01$, *** $p < .001$, **** $p < .0001$.

compounds are likely assimilated by the chondrocytes. Additionally, the presence of free hyaluronic acid induces 100% cell metabolic activity in all time points and respective concentrations indicating that HA has non-toxicity effect and is a suitable compound to keep chondrocyte cell growth levels.

3.3.2. NPs up-take by chondrocytes

To test and compare the effect of time on NPs uptake by cells, the C28/I2 cells were incubated with NPs concentration of 40 μg/mL at 37 °C and analyzed with flow cytometry and Odyssey. The frequency of FITC- positive parents and the intensity of NIR dye were measured at four time points. The up-take characterized by flow cytometry showed an increased up take over time for PLGA NPs and PLGA NPs AB, while PLGA NPs A showed a constant up take overtime (Fig. 5A). Although the graphic shows higher up-take capacity for PLGA NPs it is necessary to take into account dye EE, since the up-take seems to be dependent on EE (Table.1). The up-take graphic characterized by Odyssey showed a similar pattern. PLGA NPs (control NPs) presented a constant uptake until 4 h and an increased up-take at 24 h, while the PLGA NPs A and PLGA NPs AB showed a trend for increasing up-take over time. An optimal up-take value was observed after 4 h of incubation of PLGA NPs AB with cells (Fig. 5A, B).

To confirm the internalization of NPs, fluorescence and confocal microscopy were used to visualize the cells after 24 h of incubation. The merged images of Fig. 5C, D and E show that the NPs penetrated the cell membrane. This is further confirmed with the images of confocal microscopy (Fig. 5G, H, I). The bigger size of the green dots in the image with PLGA NPs AB (Fig. 5E) indicates that these NPs have started their release outside the cells, while the others did not (Fig. 5D). The merged images in Fig. 5C and D, which represent PLGA NPs and PLGA NPs A, respectively, show green dots, which are NPs present on the slide glass bottom, a typical phenomenon of NPs since they attach to the slide.

As expected, the burst release of the pH-responsive PLGA NPs AB is accompanied by a higher cell uptake in comparison with the non-responsive NPs already at 4 h of incubation (Fig. 5A, B). The fluorescence microscopic images (Fig. 5C- D- E) taken at the end of the first day showed intracellular release with all NPs. This extracellular release greatly contributes to cell viability since there are evidences suggesting that the HA binds to the CD44 receptor present in the cell surface activating TGF-beta 1, which in turn induces protein phosphorylation enhancing C-Myc E2F4 gene expression that is correlated with matrix regeneration [48]. Taken collectively the data indicates that the formulated pH-responsive PLGA NPs AB induced both a faster release of the encapsulated compounds and higher metabolic cell activity.

3.4. Characterization of the NPs in in vivo experiments

3.4.1. Animals osteoarthritis mouse model experiment and NPs release study in vivo

After confirming that DMM successfully induced knee OA in the mice (supplementary materials Fig. 5 A and B), the animals were treated with 3 types of NPs and followed for 35 days. A gradual decline of fluorescent signal was observed over time but still detectable *in vivo* at the latest time point (Fig. 6A). PLGA NPs AB induced a faster release of cargo than PLGA NPs and PLGA NPs A (Fig. 6). The PLGA NPs and PLGA NPs A presented a standard release curve, while PLGA NPs AB had a release peak (nearly 4 times higher than the other NPs) 24 h after administration, followed by a sharp decrease 48 h after injection with a continuing decreasing pattern over time. ANOVA indicated a statistically significant difference between the treatments ($p < .001$) (Fig. 6B). At the end of the experiment it was still possible to detect NIR dye through IVIS fluorescence imaging from the OA knee mouse treated with NPs. On the other hand, no fluorescence signal was captured from mice injected with free NIR dye (Fig. 6C). These results show that the NPs are still in the knee after 35 days of IA injection. Considering, that after 20 days of *in vitro* release study in SF the cumulative NIR dye released is a maximum of 20% (Fig. 3D), it seems possible that at 35 days the compounds loaded in NPs may still be released *in vivo*.

A collective interpretation of these and the release experiment results, (which showed that at pH 5.0, PLGA NPs AB had an initial burst release with a decrease over time, while PLGA NPs A had an initial slower release with an increase over time), indicates that combining both NPs, pH-responsive and non-pH responsive, in a single intra-articular injection in OA knee may have a synergistic effect. In this way it

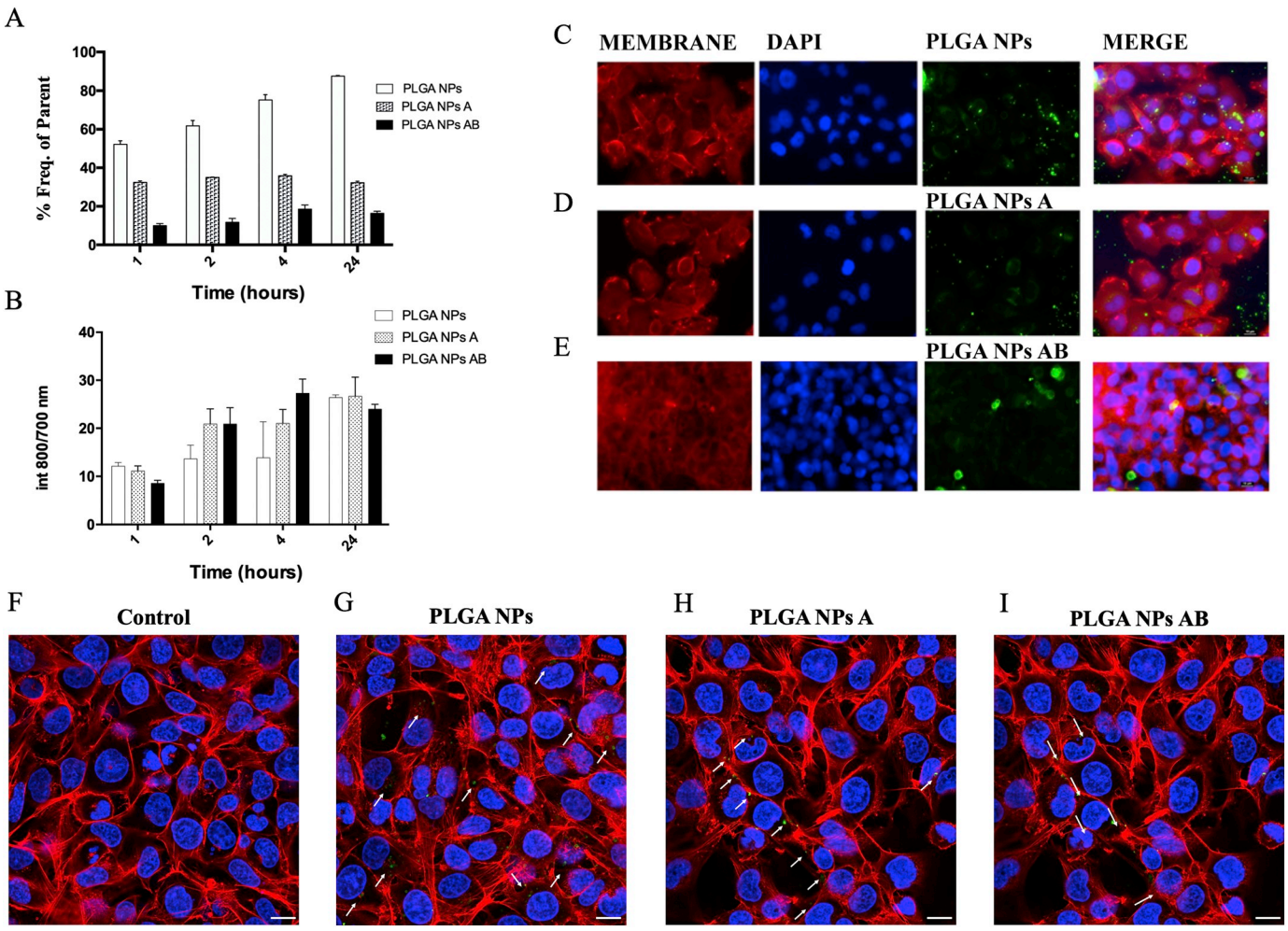

Fig. 5. Measure and visualization of C28/I2 cellular up-take of NPs. A) *In vitro* cellular up-take of PLGA NPs, PLGA NPs A and PLGA NPs AB characterized by FACS. The C28/I2 cells were incubated at 1, 2, 4 and 24 h with NPs concentration of 40 μg/mL. B) *In vitro* cellular up-take of PLGA NPs, PLGA NPs A and PLGA NPs AB characterized by Odyssey. C-D-E) Fluorescent microscopy images showing internalization of fluorescent NPs and burst release of PLGA NPs AB. Visualization after 24 h incubation in PBS of NPs. C) PLGA-NPs, D) PLGA-NPs A and E) PLGA-NPs AB. Cell membrane stained with CD44-PE (red), cell nucleus with DAPI staining (blue) and NIR NPs (green). The images were made with Leica fluorescent microscopy at 43× magnification. F- G- H– I) Confocal microscopy images. F) Only cells, no NPs treatment G) PLGA-NPs, H) PLGA-NPs A and I) PLGA-NPs AB. Phalloidin-TRITC (red), cell nucleus with DAPI (blue) and FITC NPs (green). The images were made with Leica SP8 confocal microscopy at 63× magnification. (For interpretation of the references to colour in this figure legend, the reader is referred to the web version of this article.)

is possible to achieve a faster delivery to the cells and, keep a constant and prolonged deliver of the drug to the OA tissues. This may also reduce the potential for infections after intra-articular injection treatment of viscosupplementation or anti-inflammatory drugs, since it may reduce the number of IA injections.

3.5. Characterization of the NPs in the ex vivo experiment

3.5.1. μ-CT and histological analysis

After sacrificing the mice and collecting the limbs, the legs were analyzed with μCT-scan. OA induces significant changes to the bone structure [49] therefore, μCT-scan was used to visualized the bone structure of the knee joint in each treatment group. The results show that DMM induced knee OA, since osteophytes formation and cartilage degeneration were observed in the targeted joints (Fig. 7B), while no osteophytes formations or cartilage damage were observed in healthy knees, as highlighted by the arrows in Fig. 7B. The μCT-scans of the knees treated with NPs showed minor osteophyte formations (see arrows in Fig. 7A), suggesting that PLGA NPs A and PLGA NPs AB induce a reduction in OA development. To confirm the results of the *in vivo* experiments we performed histological staining using Safranin-O to visualize the cartilage and osteophytes. The results confirm the observation obtained with the μ- CT-scan: 1) the healthy knee did not show osteophytes, 2) the OA knee with no treatment showed cartilage degeneration and osteophytes, 3) the OA knee treated with NPs showed minor osteophytes formation and cartilage damage (Fig. 7A and B). Articular damage was quantified with OARSI score (Fig. 7D and E). The sum of the average score of the medial compartment (femoral and tibia) (Fig. 7D) and the sum of the medial compartment (femoral and tibia) (Fig. 7E) per knee. Due to small sample sizes it was not possible to perform statistical analysis. Nevertheless, the OA score suggests that injection of the PLGA NPs A and AB did not worsen progression of OA in mice (Fig. 7D). Moreover, it was not possible to analyze many of the OA knee samples due to cartilage degradation and sample unsuitability for OA scoring.

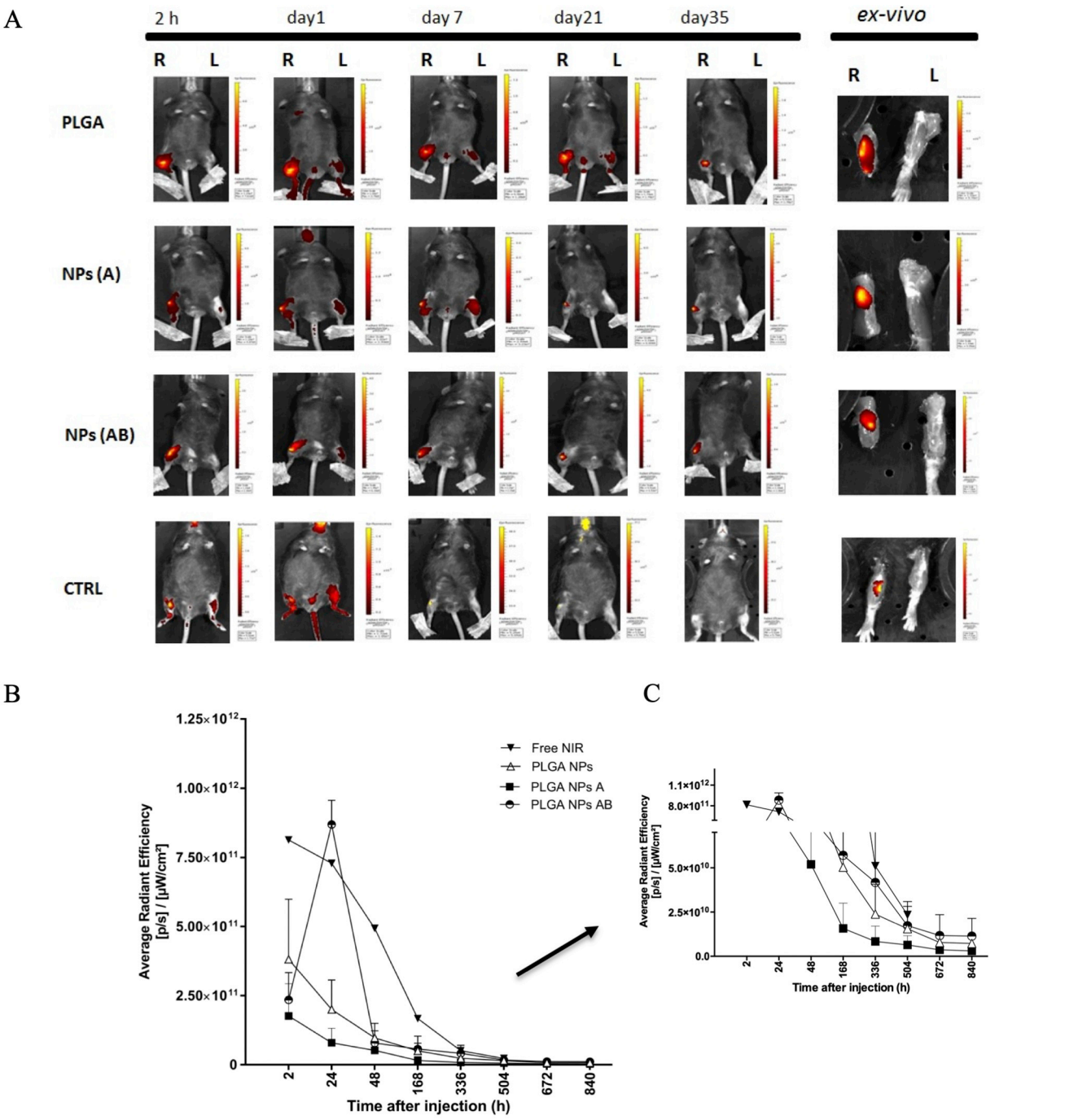

Fig. 6. A) The *in vivo* IVIS images depict a representative mouse for each NPs treatment group at 5 different time points. *Ex vivo* imaging was performed after 35 days of treatment. B) The *in vivo* retention was measured as the average radiation intensity of each NPs treatment over time, at 8 time points, in the OA knee. The control curve represents free dye injected intra-articularly and was used as a baseline comparison with the NPs. *In vivo* retention of PLGA NPs, PLGA NPs A and PLGA NPs AB co-loaded with NIR dye followed for 35 days after IA injection in the right knee. * statistical significance $p < .001$ by two-way ANOVA ($n = 4$). C) The zoom graphic of *in vivo* NPs retention in knee joint.

4. Conclusion

pH-responsive PLGA NPs AB loaded with HA and NH_4HCO_3 were successfully developed with an upcoming and promising methodology to demonstrate the efficiency in drug delivery for treatment of osteoarthritis. This study aimed at characterizing and testing the effects of pH- responsive PLGA NPs in OA nanotherapy, as well as, monitoring its effects in *in vitro* and *in vivo* experiments with molecular imaging. The results from *in vitro* and *in vivo* experiments indicate that pH-responsive NPs released the content loaded in a burst release fashion at environmental pH 5.0. Additionally, PLGA NPs AB and PLGA NPs A were not toxic to chondrocyte cells and PLGA NPs AB had no negative effects in the joint. This study points towards a high therapeutical potential by combining pH responsive with non pH-responsive NPs in a single shot it may be possible to enhance the initial pulse of drug release combining with a steady pulse of drug release.

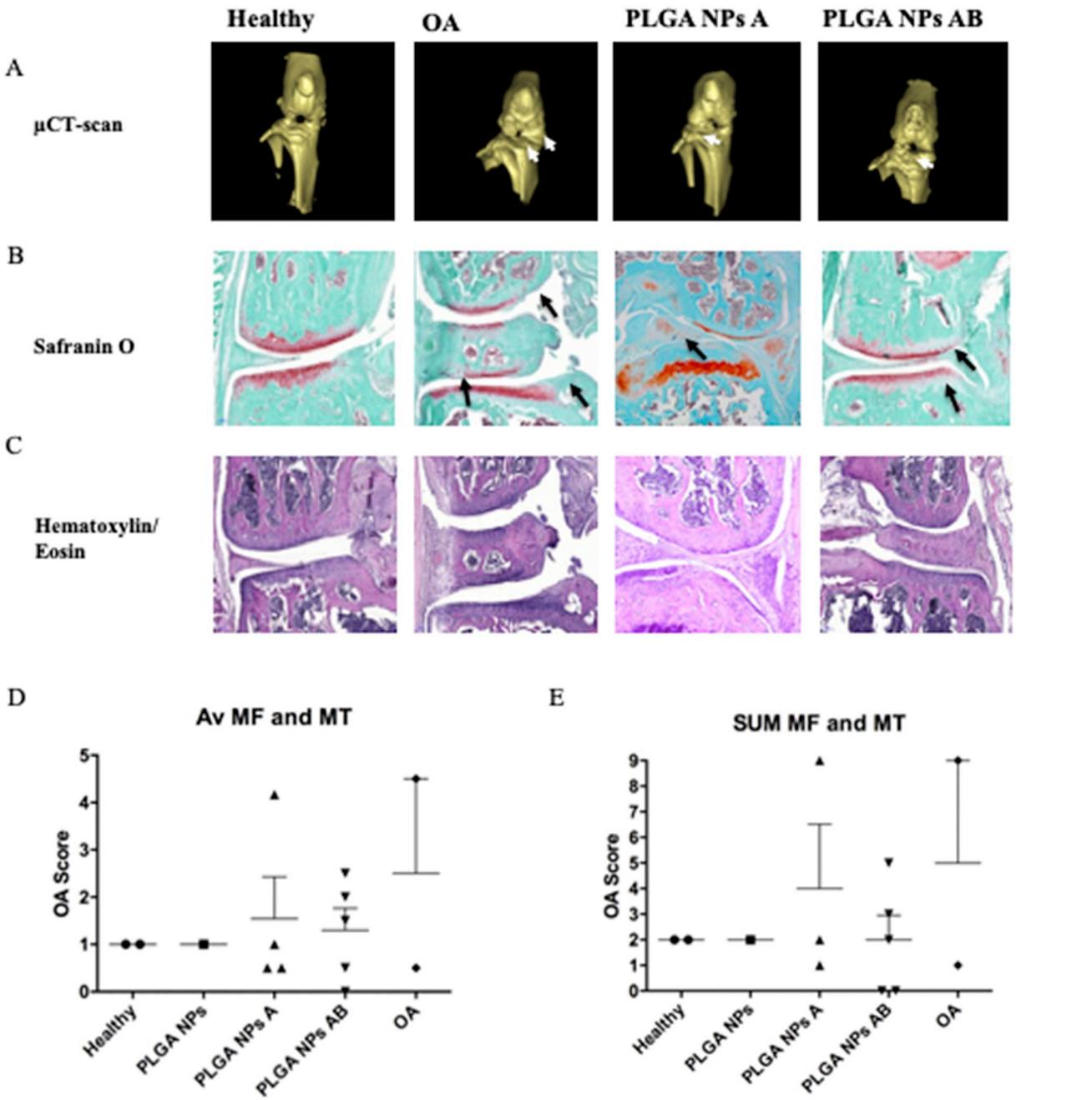

Fig. 7. Characterization of the pH-response NPs in the *ex vivo.* A) *Ex vivo* µ-CT scan of knee joints showing a 3D view of the cartilage surface. From left to right healthy knee (negative control), OA knee without NPs treatment (positive control), representative pictures of OA knee treated with PLGA NPs A and PLGA NPs AB. B) Histological staining with Safranin-O fast green, C) Hematoxylin/ Eosin staining. The arrows in µ-CT scan point to the osteophytes and in Safranin-O staining point to the damage in the cartilage and formation of osteophytes. The D) average of medial femoral condyle (MF) and medial tibial (MT) and E) sum of OA score per knee of the medial compartments (femoral and tibial). Bars represent the standard deviation (SD) of each group. (For interpretation of the references to colour in this figure legend, the reader is referred to the web version of this article.)

Acknowledgments

Authors thank PhD M. B. Goldring (Research Division, Hospital for Special Surgery, New York, USA) for providing the C28/I2 cell line, N. Kops (Department of Orthopedics, Erasmus MC University Medical Centre Rotterdam, the Netherlands) for her kind help in histology analysis. T. Schomann (Department of Otorhinolaryngology and Head & Neck Surgery; Leiden University Medical Center) for all support with fluorescence microscopy images. This work was supported by the following European Union project grants: H2020-MSCA-ITN-2014 TargetCaRe (642414), H2020-MSCA-RISE-2014 PRISAR (644373), H2020-PHC-2014-single-stage ELECTOR (643481), H2020-MSCA-ITN-2015 ISPIC (675743), H2020-MSCA-RISE-2016 CHARMED (734684) and H2020-MSCA-RISE-2017 CANCER (777682).

Appendix A. Supplementary data

Supplementary data to this article can be found online at https://doi.org/10.1016/j.jconrel.2019.07.031.

References

[1] S.R. Goldring, M.B. Goldring, Clinical aspects, pathology and pathophysiology of osteoarthritis, J. Musculoskelet. Neuronal Interact. 6 (2006) 376–378.

[2] S. Castañeda, J.A. Roman-Blas, R. Largo, G. Herrero-Beaumont, Subchondral bone as a key target for osteoarthritis treatment, Biochem. Pharmacol. 83 (2012) 315–323, https://doi.org/10.1016/j.bcp.2011.09.018.

[3] C. Buckland-Wright, Subchondral bone changes in hand and knee osteoarthritis detected by radiography, Osteoarthr. Cartil. 12 (2004) 10–19, https://doi.org/10.1016/j.joca.2003.09.007.

[4] J. Buckwalter, H. Mankin, Articular cartilage repair and transplantation, Arthritis Rheum. 41 (1998) 1331–1342, https://doi.org/10.1002/1529-0131(199808)41:8<1331::AID-ART2>3.0.CO;2-J.

[5] M. Janssen, G. Mihov, T. Welting, J. Thies, P. Emans, Drugs and polymers for delivery systems in OA joints: Clinical needs and opportunities, Polymers (Basel) (2014), https://doi.org/10.3390/polym6030799.

[6] K. Wang, J. Xu, D.J. Hunter, C. Ding, Investigational drugs for the treatment of osteoarthritis, Expert Opin. Investig. Drugs 24 (2015) 1539–1556, https://doi.org/10.1517/13543784.2015.1091880.

[7] M.M. Richards, J.S. Maxwell, L. Weng, G. Mathew, J. Golzarian, Intra-articular treatment of knee osteoarthritis: from anti-inflammatories to products of regenerative medicine, Phys. Sportsmed. 44 (2017) 101–108, https://doi.org/10.1080/00913847.2016.1168272.Intra-articular.

[8] J.R. Watterson, J.M. Esdaile, Viscosupplementation: therapeutic mechanisms and clinical potential in osteoarthritis of the knee, J. Am. Acad. Orthop. Surg. 8 (2000) 277–284, https://doi.org/10.5435/00124635-200009000-00001.

[9] T. Iannitti, D. Lodi, B. Palmieri, Intra-articular injections for the treatment of osteoarthritis: focus on the clinical use of hyaluronic acid, Drugs R D. 11 (2011) 13–27, https://doi.org/10.2165/11539760.

[10] V.B. Kraus, J.L. Huebner, J. DeGroot, A. Bendele, The OARSI histopathology initiative - recommendations for histological assessments of osteoarthritis in the Guinea pig, Osteoarthr. Cartil. (2010), https://doi.org/10.1016/j.joca.2010.04.015.

[11] U. Srejic, O. Calvillo, K. Kabakibou, Viscosupplementation: a new concept in the treatment of sacroiliac joint syndrome: a preliminary report of four cases, Reg. Anesth. Pain Med. 24 (1999) 84–88, https://doi.org/10.1016/S1098-7339(99)90170-0.

[12] H. Hempfling, Intra-articular hyaluronic acid after knee arthroscopy: a two-year study, knee surgery, Sport. Traumatol. Arthrosc. 15 (2007) 537–546, https://doi.org/10.1007/s00167-006-0260-1.

[13] R.D. Altman, A. Manjoo, A. Fierlinger, F. Niazi, M. Nicholls, The mechanism of action for hyaluronic acid treatment in the osteoarthritic knee: a systematic review, BMC Musculoskelet. Disord. 16 (2015) 1–10, https://doi.org/10.1186/s12891-015-0775-z.

[14] D. Lajeunesse, A. Delalandre, J. Martel-Pelletier, J.P. Pelletier, Hyaluronic acid reverses the abnormal synthetic activity of human osteoarthritic subchondral bone osteoblasts, Bone. 33 (2003) 703–710, https://doi.org/10.1016/S8756-3282(03)00206-0.

[15] P. Brun, B. Zavan, V. Vindigni, A. Schiavinato, A. Pozzuoli, C. Iacobellis, G. Abatangelo, *In vitro* response of osteoarthritic chondrocytes and fibroblast-like synoviocytes to a 500-730 kDa hyaluronan amide derivative, J. Biomed. Mater. Res. Part B Appl. Biomater. 100B (2012) 2073–2081, https://doi.org/10.1002/jbm.b.32771.

[16] W. Knudson, R.F. Loeser, CD44 and integrin matrix receptors participate in cartilage homeostasis, Cell. Mol. Life Sci. (2002), https://doi.org/10.1007/s00018-002-8403-0.

[17] O. Ishida, Y. Tanaka, I. Morimoto, M. Takigawa, S. Eto, Chondrocytes are regulated by cellular adhesion and hyaluronic acid pathway, J. Bone Miner. Res. 12 (1997) 1657–1663.

[18] C.B. Knudson, W. Knudson, Hyaluronan and CD44: modulators of chondrocyte metabolism, Clin. Orthop. Relat. Res. (2004) 152–162, https://doi.org/10.1097/01.blo.0000143804.26638.82.

[19] W. Knudson, B. Casey, Y. Nishida, W. Eger, K.E. Kuettner, C.B. Knudson, Hyaluronan oligosaccharides perturb cartilage matrix homeostasis and induce chondrocytic chondrolysis, Arthritis Rheum. 43 (2000) 1165–1174, https://doi.org/10.1002/1529-0131(200005)43:5<1165::AID-ANR27>3.0.CO;2-H.

[20] A.W.S. Rutjes, P. Ju, B.R. Costa, S. Trelle, E. Nu, Annals of Internal Medicine Viscosupplementation for Osteoarthritis of the Knee, (2013).

[21] V. Santilli, M. Paoloni, M. Mangone, F. Alviti, A. Bernetti, Hyaluronic acid in the management of osteoarthritis: Injection therapies innovations, Clin. Cases Miner. Bone Metab. 13 (2016) 131–134, https://doi.org/10.11138/ccmbm/2016.13.2.131.

[22] F. Rannou, J.P. Pelletier, J. Martel-Pelletier, Efficacy and safety of topical NSAIDs in the management of osteoarthritis: evidence from real-life setting trials and surveys, Semin. Arthritis Rheum. 45 (2016) S18–S21, https://doi.org/10.1016/j.semarthrit.2015.11.007.

[23] K.A. Campbell, B.J. Erickson, B.M. Saltzman, R. Mascarenhas, B.R. Bach, B.J. Cole, N.N. Verma, Is local Viscosupplementation injection clinically superior to other therapies in the treatment of osteoarthritis of the knee: a systematic review of overlapping meta-analyses, Arthroscopy. 31 (2015) 2036–2045, https://doi.org/10.1016/j.arthro.2015.03.030.

[24] M.E. Adams, A.J. Lussier, J.G. Peyron, A risk-benefit assessment of injections of hyaluronan and its derivatives in the treatment of osteoarthritis of the knee, Drug Saf. 23 (2000) 115–130, https://doi.org/10.2165/00002018-200023020-00003.

[25] H. Zille, J. Paquet, C. Henrionnet, J. Scala-Bertola, M. Leonard, J.L. Six, F. Deschamp, P. Netter, J. Vergès, P. Gillet, L. Grossin, Evaluation of intra-articular delivery of hyaluronic acid functionalized biopolymeric nanoparticles in healthy rat knees, Biomed. Mater. Eng. 20 (2010) 235–242, https://doi.org/10.3233/BME-2010-0637.

[26] R.E. Whitmire, D. Scott Wilson, A. Singh, M.E. Levenston, N. Murthy, A.J. García, Self-assembling nanoparticles for intra-articular delivery of anti-inflammatory proteins, Biomaterials. 33 (2012) 7665–7675, https://doi.org/10.1016/j.biomaterials.2012.06.101.

[27] X. Yu, I. Trase, M. Ren, K. Duval, X. Guo, Z. Chen, Design of nanoparticle-based carriers for targeted drug delivery, J. Nanomater. (2016), https://doi.org/10.1155/2016/1087250.

[28] J.-M. Lu, X. Wang, C. Marin-Muller, H. Wang, P.H. Lin, Q. Yao, C. Chen, Current advances in researcn and clinical applications of PLGA-based nanotechnology, Expert. Rev. Mol. Daign. 9 (2009) 325–341, https://doi.org/10.1586/erm.09.15.Current.

[29] U.D. Bret, N.S. Lakshmi, C.T. Laurencin, Biomedical applications of biodegradable polymers, J. Polym. Sci. Part B Polym. Phys. 3 (2011) 832–864, https://doi.org/10.3390/polym3031377.Poly.

[30] Z. Chen, J. Chen, L. Wu, W. Li, J. Chen, H. Cheng, J. Pan, B. Cai, Hyaluronic acid-coated bovine serum albumin nanoparticles loaded with brucine as selective nanovectors for intra-articular injection, Int. J. Nanomedicine 8 (2013) 3843–3853, https://doi.org/10.2147/IJN.S50721.

[31] Z. Chen, D. Liu, J. Wang, L. Wu, W. Li, J. Chen, B.C. Cai, H. Cheng, Development of nanoparticles-in-microparticles system for improved local retention after intra-articular injection, Drug Deliv. 21 (2014) 342–350, https://doi.org/10.3109/10717544.2013.848495.

[32] M. Farr, K. Garvey, A.M. Bold, M.J. Kendall, P.A. Bacon, Significance of the hydrogen ion concentration in synovial fluid in rheumatoid arthritis, Clin. Exp. Rheumatol. 3 (1985) 99–104 http://www.vivalis.si/uploads/datoteke/7a95.pdf.

[33] Q. Liu, X. Chen, J. Jia, W. Zhang, T. Yang, L. Wang, G. Ma, PH-responsive poly(D,L-lactic-co-glycolic acid) nanoparticles with rapid antigen release behavior promote immune response, ACS Nano (2015), https://doi.org/10.1021/nn5066793.

[34] R.A. Rosalia, L.J. Cruz, S. van Duikeren, A.T. Tromp, A.L. Silva, W. Jiskoot, T. de Gruijl, C. Löwik, J. Oostendorp, S.H. van der Burg, F. Ossendorp, CD40-targeted dendritic cell delivery of PLGA-nanoparticle vaccines induce potent anti-tumor responses, Biomaterials. 40 (2015) 88–97, https://doi.org/10.1016/j.biomaterials.2014.10.053.

[35] N. Oueslati, P. Leblanc, C. Harscoat-Schiavo, E. Rondags, S. Meunier, R. Kapel, I. Marc, CTAB turbidimetric method for assaying hyaluronic acid in complex environments and under cross-linked form, Carbohydr. Polym. 112 (2014) 102–108, https://doi.org/10.1016/j.carbpol.2014.05.039.

[36] M.B. Goldring, J.R. Birkhead, L. Suen, R. Yamin, S. Mizuno, J. Glowacki, J.L. Arbiser, J.F. Apperleyll, Human Chondrocytes 94 (1994) 2307–2316.

[37] H. Claassen, M. Schicht, J. Brandt, K. Reuse, R. Schädlich, M.B. Goldring, S.S. Guddat, A. Thate, F. Paulsen, C-28/I2 and T/C-28a2 chondrocytes as well as human primary articular chondrocytes express sex hormone and insulin receptors-useful cells in study of cartilage metabolism, Ann. Anat. (2011), https://doi.org/10.1016/j.aanat.2010.09.005.

[38] S.S. Glasson, T.J. Blanchet, E.A. Morris, The surgical destabilization of the medial meniscus (DMM) model of osteoarthritis in the 129/SvEv mouse, Osteoarthr. Cartil. (2007), https://doi.org/10.1016/j.joca.2007.03.006.

[39] S. Khatab, G.M. van Buul, N. Kops, Y.M. Bastiaansen-Jenniskens, P.K. Bos, J.A. Verhaar, G.J. van Osch, Intra-articular injections of platelet-rich plasma Releasate reduce pain and synovial inflammation in a mouse model of osteoarthritis, Am. J. Sports Med. 46 (2018) 977–986, https://doi.org/10.1177/0363546517750635.

[40] R. Singh, J.W. Lillard, Nanoparticle-based targeted drug delivery, Exp. Mol. Pathol. 86 (2009) 215–223, https://doi.org/10.1016/j.yexmp.2008.12.004.Nanoparticle-based.

[41] K.S.K. Soppimath, T.M.T.M. Aminabhavi, A.R.A.R. Kulkarni, W.E. Rudzinski, Biodegradable polymeric nanoparticles as drug delivery devices, J. Control. Release 70 (2001) 1–20, https://doi.org/10.1016/S0168-3659(00)00339-4.

[42] B. Magenheim, M.Y. Levy, S. Benita, A new in vitro technique for the evaluation of drug release profile from colloidal carriers - ultrafiltration technique at low pressure, Int. J. Pharm. 94 (1993) 115–123, https://doi.org/10.1016/0378-5173(93)90015-8.

[43] L. Shang, K. Nienhaus, G.U. Nienhaus, Engineered nanoparticles interacting with cells: size matters, J. Nanobiotechnol. 12 (2014) 1–11, https://doi.org/10.1186/1477-3155-12-5.

[44] E. Fröhlich, The role of surface charge in cellular uptake and cytotoxicity of medical nanoparticles, Int. J. Nanomedicine 7 (2012) 5577–5591, https://doi.org/10.2147/IJN.S36111.

[45] V. Ayala, A.P. Herrera, M. Latorre-Esteves, M. Torres-Lugo, C. Rinaldi, Effect of surface charge on the colloidal stability and in vitro uptake of carboxymethyl dextran-coated iron oxide nanoparticles, J. Nanopart. Res. 15 (2013) 1–24, https://doi.org/10.1007/s11051-013-1874-0.

[46] S. Bhattacharjee, DLS and zeta potential - what they are and what they are not? J. Control. Release 235 (2016) 337–351, https://doi.org/10.1016/j.jconrel.2016.06.017.

[47] A. Kumari, S.K. Yadav, S.C. Yadav, Biodegradable polymeric nanoparticles based drug delivery systems, Colloids Surfaces B Biointerfaces. 75 (2010) 1–18, https://doi.org/10.1016/j.colsurfb.2009.09.001.

[48] D.J. Responte, R.M. Natoli, K.A. Athanasiou, Identification of potential biophysical and molecular signalling mechanisms underlying hyaluronic acid enhancement of cartilage formation, J R Soc Interface (2012) 3564–3573.

[49] T. Neogi, Clinical significance of bone changes in osteoarthritis, Ther. Adv. Musculoskelet. Dis. 4 (2012) 259–267, https://doi.org/10.1177/1759720X12437354.